PROCEEDINGS OF SCIENCE

Particle identification in KM3NeT/ORCA

L. Cerisy,[a,*] A. Lazo,[b] C. Lastoria,[a] M. Perrin-Terrin,[a] J. Brunner[a] and V. Dabhi[a,1] on behalf of the KM3NeT collaboration

[a] *Aix Marseille Univ, CNRS/IN2P3, CPPM, Marseille, France*

[b] *IFIC - Instituto de Física Corpuscular (CSIC - Universitat de València), c/Catedrático José Beltrán, 2, 46980 Paterna, Valencia, Spain*

[1] *Not a KM3NeT member, contributed during his master thesis*

E-mail: cerisy@cppm.in2p3.fr

One of the main goals of KM3NeT/ORCA is to measure atmospheric neutrino oscillation parameters with competitive precision. To achieve this goal, good discrimination between track-like and shower-like events is necessary, with particular focus on the measurement of the tau neutrino normalisation. The track-like signal is mainly carried by muon neutrinos from charged current interactions, while the shower-like signal comes from charged current interactions of electron and tau neutrinos, and neutral current interactions of all flavours. A Random Grid Search algorithm is optimised to separate these channels and its performance is compared with machine learning methods using boosted decision trees. This contribution will report on the technical aspects of the algorithm and the performance of the particle identification with data recorded in 2020 and 2021 using an early six-lines configuration of the ORCA detector (ORCA6).

38th International Cosmic Ray Conference (ICRC2023)
26 July - 3 August, 2023
Nagoya, Japan

*Speaker

PoS(ICRC2023)1191

1. Introduction

Particle identification plays a crucial role in most neutrino studies aimed at measuring flavour oscillations with high precision. This contribution reports on the track-shower separation to identify neutrino flavours using the KM3NeT/ORCA6 data, with a particular focus on the optimisation of the ν_τ appearance signal. The track-like signal refers to the muon from the charged current muon neutrino interaction. The shower-like signal refers to the electro-magnetic(EM) shower from the charged current electron neutrino interaction, the EM/hadronic shower from the charged current tau neutrino interaction, and the hadronic shower from the neutral current channel for all-flavors. With a still size-limited detector, no significant separability between electro-magnetic and hadronic shower is expected.

Sophisticated methods are being explored to perform particle identification such as Boosted Decision Trees (BDTs), used in the official KM3NeT/ORCA results, and most recently Deep Neural Networks (DNN). While these approaches show a strong potential to find the purest classification, new ideas to improve the robustness against mismodelling effects from the simulations and the understanding of the parameters used for particle identification, are described in this contribution.

The Random Grid Search (RGS) algorithm consist in a transparent and robust approach that relies on a combination of cuts in one or two dimension to separate two (or more) populations of events. A strong advantage of this method is the ability to look for the reasons why a particular data sample was chosen. By using a combination of cuts that involve a few features (typically 4 or 5) one can investigate the data/MC agreement and interpret the physical meaning of the features.

2. Detector and data sample

KM3NeT is an undersea Cherenkov neutrino telescope currently under construction at the bottom of the Mediterranean Sea off-shore the Italian Sicily coast (KM3NeT/ARCA) and 40 km off-shore Toulon, France (KM3NeT/ORCA). The two detectors are optimised for different neutrino energy ranges. They are composed of vertical Detection Units (DUs), each consisting of 18 Digital Optical Modules (DOMs). A DOM is housing 31 photomultiplier tubes (PMTs) and the corresponding readout electronics. Six DUs were operational in KM3NeT/ORCA when the data used in this analysis were acquired. A hit consists of a time stamp and a time over threshold. An event is created when the trigger algorithm identifies a series of causally-connected hits. The vertex position, the time and the direction of the event is determined by using a maximum-likelihood method based on a set of causally-connected hit times and positions. For the track reconstruction the hits are fitted under the assumption of a Cherenkov-light-emitting muon. The muon is assumed to follow a long, straight trajectory and to propagate practically at the speed of light in vacuum through water. For the shower reconstruction the signal is searched in all direction within 80m from the shower vertex pre-fit position, the hits are fitted to find the brightest point of the shower, expected a few meters from the neutrino vertex position depending on energy.

The data used in this analysis were collected between mid-February 2020, and mid-November 2021 for a total of 510 days or 433 kton-years. Quality cuts on the number of used hits >= 15, the likelihood >= 40 and the direction (up-going) of the track reconstruction were applied to remove poorly reconstructed events, noise events from K40 decay, and most of the atmospheric muon background. A cut keeping events below 100GeV in the energy from the track reconstruction is applied to the Tracks class (defined in Section 3) and 1TeV from the shower reconstruction energy to the Showers class to remove high energy events migration.

3. BDT Performance

A BDT based algorithm is used in the official oscillation analysis and relies on the training of the classifier on 45 different features using unweighted MC events. Those features are related to the energy, likelihood of the track/shower reconstruction, direction, hits of each reconstructed event. The trained classifier applied to a sample predicts a Track score and an atmopsheric muon (Atm. muon) score that determines the likeliness of an event to be associated to a **muon neutrino** or an **atmospheric muon**, respectively. In Figure 1 the weighted distribution of the scores and the data/MC ratio illustrates the good agreement between data and expectation for those variables.

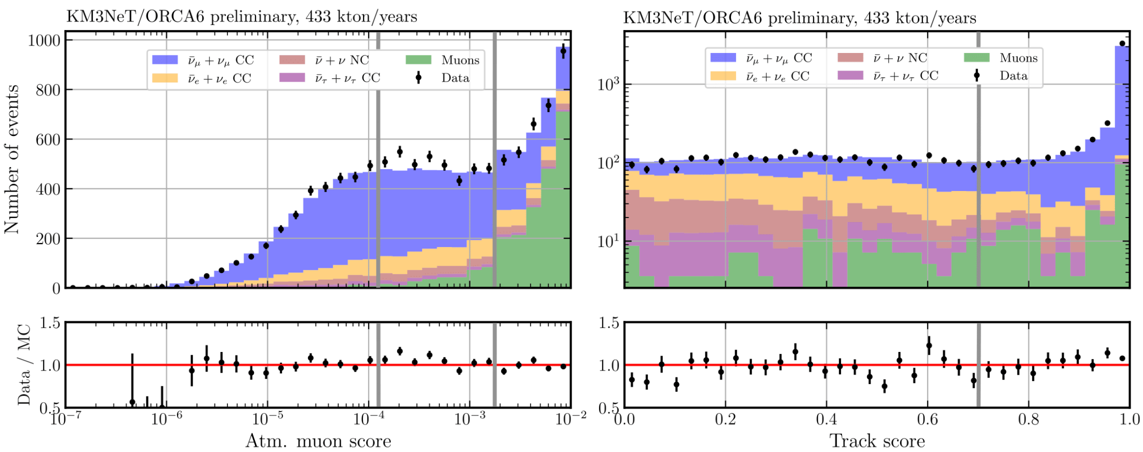

Figure 1: The Atmospheric muon score and Track score stacked distribution for all neutrino flavors is drawn in colors with atmospheric muons in green, $\nu_\tau + \bar{\nu}_\tau$ CC in purple, $\nu + \bar{\nu}$ NC in brown, $\nu_e + \bar{\nu}_e$ CC in orange and $\nu_\mu + \bar{\nu}_\mu$ CC in blue. The Data is shown with black dots and error bars. On the bottom part the data/MC ratio shows the agreement between the expected number of events and the collected data. The grey bands represents the cut values used to defined the classes.

To measure neutrino oscillations, a clean neutrino sample is produced by further removing the atmospheric muon background that passed the upgoing direction selection with a cut on the Atm. muon score at $1.8 * 10^{-3}$. In this approach the BDT outputs are also used to separate the data into three classes. The events that have a Track score below 0.7 are classified as Showers, while the events that fall above 0.7 are further divided into 2 classes the High and Low Purity Tracks by cutting on the Atm. muon score at $1.1 * 10^{-4}$. The cuts in the BDT scores have been optimised for performance to measure neutrino oscillation parameters [1]. Each class is defined to ensure enough statistics per class and per bin. The Table 1 shows the statistics contained in each class, the % of muons, $\nu_\mu/\bar{\nu}_\mu$ CC and $\nu_\tau/\bar{\nu}_\tau$ CC, for 433 kton-years and 296 kton-years samples.

Selection	All events	Atm. muons	$\nu_\mu/\bar{\nu}_\mu$ CC	$\nu_\tau/\bar{\nu}_\tau$ CC
High Purity Tracks	1870	7	1779	20
Low Purity Tracks	2001	83	1792	18
Showers	1959	21	908	130
433 kton-years	5830	111	4480	169
296 kton-years	1250	38	900	65

Table 1: Summary of the number of MC events for the different classes defined by the BDT separation. The exposure for ICRC 2023 is 433 kton-years, while the exposure for ICRC21 is 296 kton-years. The muon contamination is given as the number of atmospheric muons divided by the number of total events. The % of $\nu_\mu/\bar{\nu}_\mu$ CC events and number of $\nu_\tau/\bar{\nu}_\tau$ is also written to illustrate the purity of the classes.

4. Random Grid Search

The Random Grid Search algorithm was introduced in 1995 during the search of the top quark at FermiLab [2], and is still used in multiple experiments like in the search for supersymmetry at LHC [3].

The RGS procedure starts with the ranking of the features using weighted events from the track and shower reconstructions based on their 2D separability that measures the overlap between the track ($\nu_\mu + \bar{\nu}_\mu$ CC) and the shower ($\nu_e + \bar{\nu}_e$ CC) distribution. As a second step the 2D asymmetry and the data/MC agreement for the best ranked features are investigated to verify the understanding of the features. Then the RGS algorithm is applied, with the idea to search for cuts where they are likely to be useful, i.e. in the expected signal region. If events $E_0...E_n$ represent neutrino interactions, with for instance a direction and and position which are called features X and Y then $(E_0(X_0), E_0(Y_0))...(E_n(X_n), E_n(Y_n))$ can be used to cut the sample in two. A combination of consecutive cuts for a given event E_i with $0 \leq i \leq n$ in 1D like $((E_i(X_i), >), (E_i(Y_i), <))$ is called a set of cuts. By keeping track of the signal events (true positive rate) and background events (false positive rate) that passed the set of cuts, the performance graph shown in Figure 2 is produced. The RGS tests all the sets of cuts in 2D based on a fixed set of features. After comparing the best sets of cuts for many different sets of features, the best set of features is fixed.

Once the best set of features is fixed, the optimisation stage starts in order to find the best cut values which would give the highest sensitivity for a given study. In this work the purpose was to increase the sensitivity to ν_τ appearance [4]. It was found that the best classes division for ν_τ appearance observation was into 3 classes: track, mixed and showers without separating in this approach the track class into 2 as this has no effect on the ν_τ appearance sensitivity. In this approach the events that have an Atm. muon score below $3 * 10^{-3}$ are kept. In Figure 3 the red lines represents the optimised 2D combination A & B that define the RGS track class. The mixed+showers region is further divided in two classes thanks to the intersection of the 2D combination C & D & F written in Table 2.

A Cherenkov hit is defined as a hit whose closest distance from the track is below 100 meters and whose time is within ±15 ns range from the expected time of the hit following the Cherenkov hypothesis. The definition of the features shown in Figure 4 are reported here from left to right and top to bottom. 1 - number of reconstructed tracks within 1° from the best track. 2 - the furthest Cherenkov hit distance to the start of the track in meters, and zero for the events that do not have any Cherenkov hits. 3 - the mean of the absolute value of the time residuals of the hits within 10°

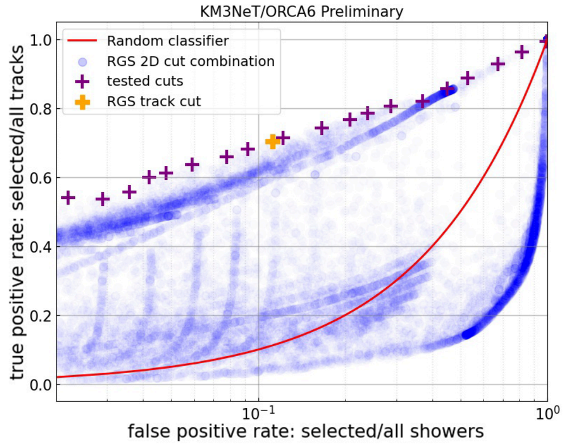

Figure 2: Efficiency and purity of each of the RGS sets of cuts. Those are shown with blue dots, while the tested cut values for optimisation are shown with purple crosses. The orange cross represents the chosen value for the RGS cut for track isolation after optimisation of the sensitivity to ν_τ appearance. A random classifier is shown with a red line for comparison.

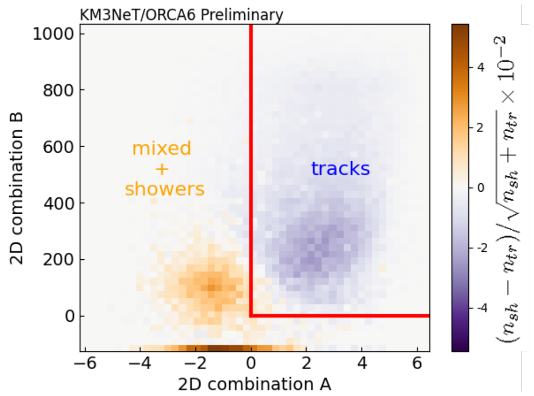

Figure 3: Significance of the track-shower asymmetry, with n_{sh} and n_{tr} the number of showers and tracks in each bin respectively. The blue region is enhanced in tracks while the orange region is enhanced in showers. Red lines are used to define the separation between the Tracks class and the Showers+Mixed classes by the RGS cuts defined in Table 2.

around the Cherenkov angle assuming the best track direction from the shower reconstruction. 4 - the log of the distance between shower reco vertex and the start of the track propagated in the track direction from a distance corresponding to the time difference of the two reconstructions at the speed of light in vacuum. 5 - the distance between the shower reco pre-reconstructed vertex and the position of the brightest point of the shower after the position fit.

In the data/MC comparison for the 5 features involved in the RGS cuts, the events corresponding to all MC flavors are weighted, this allows to appreciate the good understanding of the data for each parameter that is used in the RGS class separation. For most bins the data/MC ratios are contained in a ±20% band around 1. The peak at 0 in the parameter showing the distance to the furthest Cherenkov hit correspond to events for which no hit passes the Cherenkov distance and time conditions.

2D combination $Z = y - (ax + b)$					
RGS track class definition: $A\&B$					
pars.	feature x	feature y	coeff a	coeff b	cut dir.
comb. A	n. tracks within 1°	log pre/pos fit dist. Shower Reco	-0.2356	+ 1.9124	$Z > 0$
comb. B	furthest Cherenkov hit	mean time residual of sel. hits	-5.0702	+125.6146	$Z > 0$
RGS shower class definition: $(\bar{A} or \bar{B})$ & $(C\&D\&F)$					
comb. C	log pre/pos fit dist. Shower Reco	furthest Cherenkov hit	-0.0101	+71.1553	$Z < 0$
comb. D	log pre/pos fit dist. Shower Reco	mean time residual of sel. hits	-3.0422	+7.4538	$Z < 0$
comb. E	mean time residual of sel. hits	log dist. Shower vs Track reco	-0.3291	+2.503	$Z < 0$

Table 2: Coefficients of RGS cut combination for Tracks and Showers classes definition.

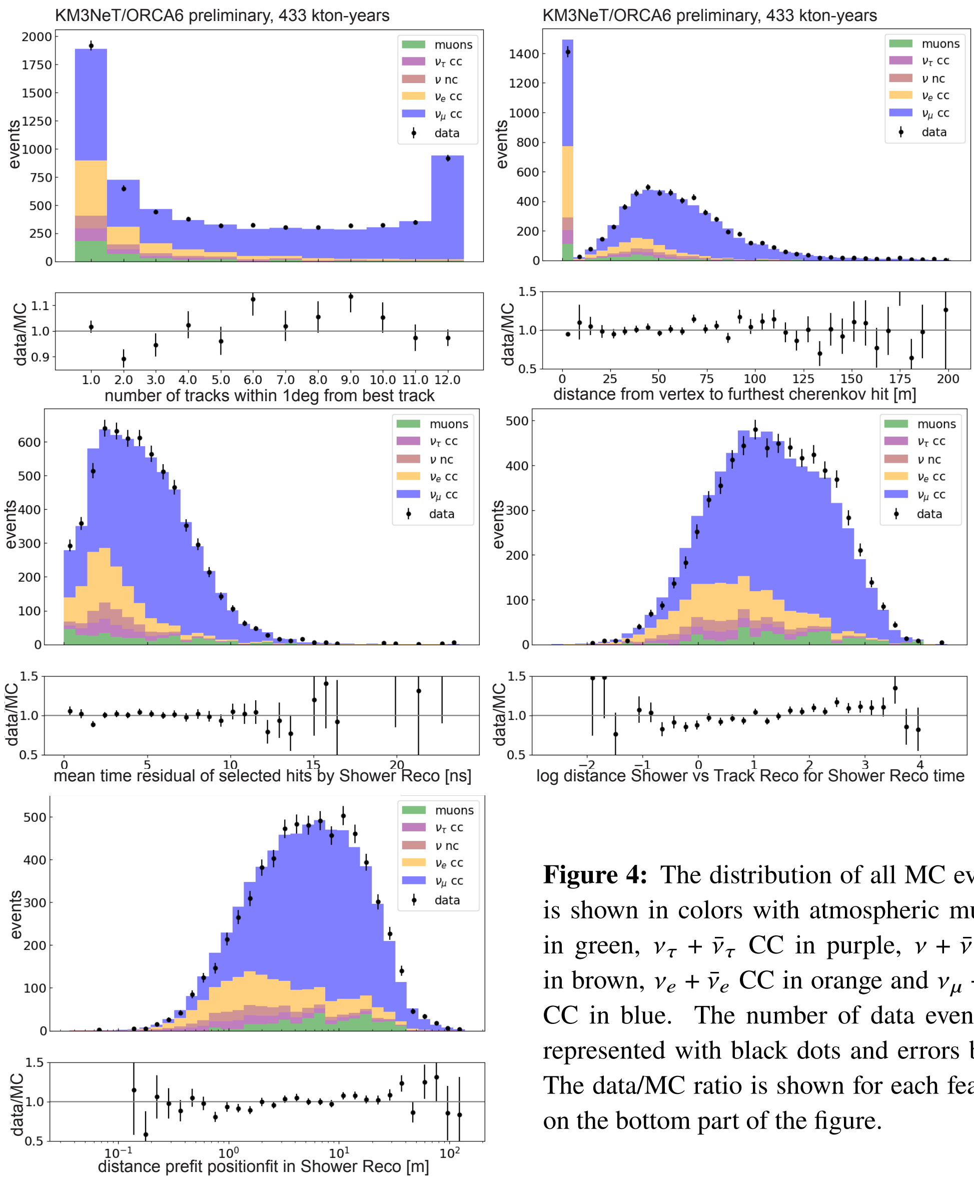

Figure 4: The distribution of all MC events is shown in colors with atmospheric muons in green, $\nu_\tau + \bar{\nu}_\tau$ CC in purple, $\nu + \bar{\nu}$ NC in brown, $\nu_e + \bar{\nu}_e$ CC in orange and $\nu_\mu + \bar{\nu}_\mu$ CC in blue. The number of data events is represented with black dots and errors bars. The data/MC ratio is shown for each feature on the bottom part of the figure.

5. Tau appearance sensitivity

After being completed, the full KM3NeT/ORCA detector is expected to measure 3000 ν_τ per year. As a comparison IceCube DeepCore measured in 1022 days for their Analysis B, 934 $\nu_\tau + \bar{\nu}_\tau$ CC, 3368 $\nu_\mu + \bar{\nu}_\mu$ CC and 1889 atmospheric muons [5]. As the typical ν_τ energy is close to 25GeV, above KM3NeT/ORCA energy threshold, it will already be sensitive to ν_τ appearance at a primary stage of construction [6]. For the moment the ν_τ are measured as an excess in the shower class. The RGS cuts presented in this work were optimised to define classes in order to have the highest possible sensitivity to ν_τ appearance.

For each of the 3 classes defined previously the oscillation parameters are fitted in the 2D space of the reconstructed zenith angle and the reconstructed energy. The fit is accounting for various systematic effects reported in [1]. The ν_τ normalisation is unconstrained in this study.

The sensitivity to tau appearance is shown in Figure 5. The comparison is made between the two separation methods discussed in this work, in the CC-only case where the ν_τ normalisation affects only the events rates in the charged current interaction channel and in the CC+NC case where the ν_τ normalisation affects event rates in both interaction channels. The sensitivity using both separation methods is similar, and indicates that the no ν_τ hypothesis could be significantly rejected with this data set if data matches expectations.

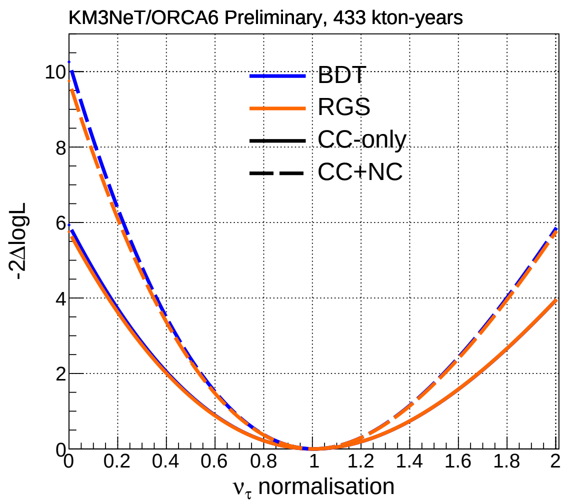

Figure 5: Sensitivity to ν_τ normalisation corresponding to the ICRC23 433 kton-years data sample when using RGS (in orange) and BDT (in blue) methods for particle identification of tracks and showers. The full line represents the ν_τ normalisation affecting CC-only and the dotted line both CC+NC events.

Figure 6 contains the reconstructed L/E distribution which combines the two main observables, the reconstructed zenith angle and the reconstructed energy of the neutrinos. The L/E distribution offers a good visibility of the oscillation dip in both the Tracks and Showers classes. The Shower reconstruction is used for the Showers and Mixed classes and the Track reconstruction is used for the Tracks class from RGS and the Low/High Purity Tracks as well. The BDT classification is used on the left plots and the RGS classification for the right plots. The top histograms show the BDT High Purity Tracks class/RGS Tracks class while the lower ones show the Showers class for both. The left histograms reveals the result of the fit with different hypothesis, free ν_τ normalisation, fixed to 0 for the no-τ hypothesis and fixed to 1 for the nominal ν_τ hypothesis. The best fit lies in the middle of the two hypothesis 0 and 1. On the other side one can appreciate the L/E range between the 2 hypothesis when using the RGS classification without showing the best fit. Data point are shown in blacks only for the official result, where the oscillation gap is clearly visible. More data will be needed to measure significantly the tau appearance, while high ν_τ normalisation are already rejected by the measurement from KM3NeT [4].

From preliminary studies, using the RGS classification allows for a better agreement between the fitted model and the data, compared to the official BDT classification. However, further studies are ongoing in order to investigate the differences between the two approaches and identify how to improve particle identification.

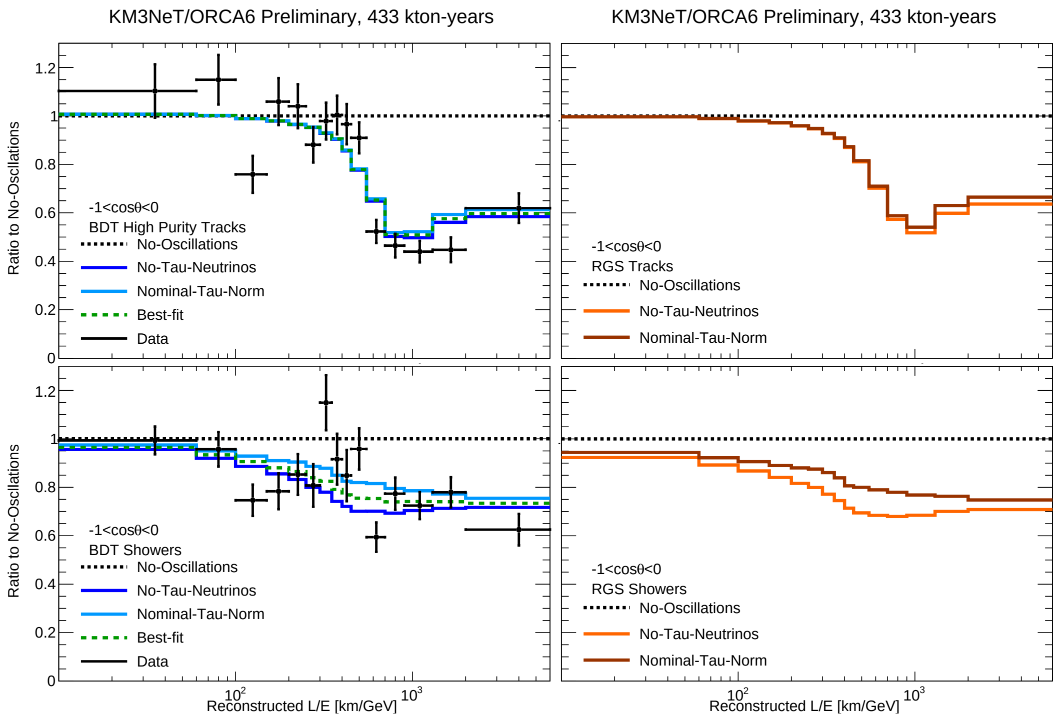

Figure 6: The L/E distributions of data and MC for different hypotheses are shown. The L/E using BDT classification is shown on the left side and the RGS classification on the right side. On the top the BDT High Purity Tracks class/RGS Tracks class is represented while on the lower part the BDT/RGS Showers classes are shown. One the left histograms the result of the fit with free ν_τ normalisation is drawn in green, the no-τ hypothesis in blue and nominal ν_τ normalisation hypothesis in cyan. In the right part the no-τ and nominal ν_τ normalisation hypothesis are drawn in orange and brown respectively.

6. Conclusion

This work highlights the potential for a new particle identification method that relies on a few features and gives a similar sensitivity to ν_τ appearance as the BDT classification. The good understanding of our data was demonstrated in the different comparisons between data and MC for the features involved in both methods. Many new possibilities in the particle identification will arise as the detector grows. One of them is the direct identification of ν_τ CC in the Showers class.

References

[1] V. Carretero, PoS(ICRC2023)996 (2023)

[2] F. Abe, et al., Phys. Rev. Lett. **74**, 2626 (1995). DOI 10.1103/PhysRevLett.74.2626

[3] P.C. Bhat, H.B. Prosper, S. Sekmen, C. Stewart, Comp. Phys. Com. **228**, 245 (2018). DOI 10.1016/j.cpc.2018.02.018

[4] N. Geisselbrecht, PoS(ICRC2023)1107 (2023)

[5] M.G. Aartsen, et al., Physical Review D **99**(3) (2019). DOI 10.1103/physrevd.99.032007

[6] R.M. Abraham, et al., Journal of Physics G: Nuclear and Particle Physics **49**(11), 110501 (2022). DOI 10.1088/1361-6471/ac89d2

PoS(ICRC2023)1191

Full Authors List: The KM3NeT Collaboration

S. Aiello[a], A. Albert[b,bd], S. Alves Garre[c], Z. Aly[d], A. Ambrosone[f,e], F. Ameli[g], M. Andre[h], E. Androutsou[i], M. Anguita[j], L. Aphecetche[k], M. Ardid[l], S. Ardid[l], H. Atmani[m], J. Aublin[n], L. Bailly-Salins[o], Z. Bardačová[q,p], B. Baret[n], A. Bariego-Quintana[c], S. Basegmez du Pree[r], Y. Becherini[n], M. Bendahman[m,n], F. Benfenati[t,s], M. Benhassi[u,e], D.M. Benoit[v], E. Berbee[r], V. Bertin[d], S. Biagi[w], M. Boettcher[x], D. Bonanno[w], J. Boumaaza[m], M. Bouta[y], M. Bouwhuis[r], C. Bozza[z,e], R.M. Bozza[f,e], H.Brânzaş[aa], F. Bretaudeau[k], R. Bruijn[ab,r], J. Brunner[d], R. Bruno[a], E. Buis[ac,r], R. Buompane[u,e], J. Busto[d], B. Caiffi[ad], D. Calvo[c], S. Campion[g,ae], A. Capone[g,ae], F. Carenini[t,s], V. Carretero[c], T. Cartraud[n], P. Castaldi[af,s], V. Cecchini[c], S. Celli[g,ae], L. Cerisy[d], M. Chabab[ag], M. Chadolias[ah], A. Chen[ai], S. Cherubini[aj,w], T. Chiarusi[s], M. Circella[ak], R. Cocimano[w], J.A.B. Coelho[n], A. Coleiro[n], R. Coniglione[w] P. Coyle[d], A. Creusot[n], A. Cruz[al], G. Cuttone[w], R. Dallier[k], Y. Darras[ah], A. De Benedittis[e], B. De Martino[d], V. Decoene[k], R. Del Burgo[e], U.M. Di Cerbo[e], L.S. Di Mauro[w], I. Di Palma[g,ae], A.F. Díaz[j], C. Diaz[j], D. Diego-Tortosa[w], C. Distefano[w], A. Domi[ah], C. Donzaud[n], D. Dornic[d], M. Dörr[am], E. Drakopoulou[i], D. Drouhin[b,bd], R. Dvornický[q], T. Eberl[ah], E. Eckerová[q,p], A. Eddymaoui[m], T. van Eeden[r], M. Eff[n], D. van Eijk[r], I. El Bojaddaini[y], S. El Hedri[n], A. Enzenhöfer[d], G. Ferrara[w], M. D. Filipović[an], F. Filippini[t,s], D. Franciotti[w], L.A. Fusco[z,e], J. Gabriel[ao], S. Gagliardini[g], T. Gal[ah], J. García Méndez[l], A. Garcia Soto[c], C. Gatius Oliver[r], N. Geißelbrecht[ah], H. Ghaddari[y], L. Gialanella[e,u], B.K. Gibson[v], E. Giorgio[w], I. Goos[n], D. Goupilliere[o], S.R. Gozzini[c], R. Gracia[ah], K. Graf[ah], C. Guidi[ap,ad], B. Guillon[o], M. Gutiérrez[aq], H. van Haren[ar], A. Heijboer[r], A. Hekalo[am], L. Hennig[ah], J.J. Hernández-Rey[c], F. Huang[d], W. Idrissi Ibnsalih[e], G. Illuminati[s], C.W. James[al], M. de Jong[as,r], P. de Jong[ab,r], B.J. Jung[r], P. Kalaczyński[at,be], O. Kalekin[ah], U.F. Katz[ah], N.R. Khan Chowdhury[c], A. Khatun[q], G. Kistauri[av,au], C. Kopper[ah], A. Kouchner[aw,n], V. Kulikovskiy[ad], R. Kvatadze[av], M. Labalme[o], R. Lahmann[ah], G. Larosa[w], C. Lastoria[d], A. Lazo[c], S. Le Stum[d], G. Lehaut[o], E. Leonora[a], N. Lessing[c], G. Levi[t,s], M. Lindsey Clark[n], F. Longhitano[a], J. Majumdar[r], L. Malerba[ad], F. Mamedov[p], J. Mańczak[c], A. Manfreda[e], M. Marconi[ap,ad], A. Margiotta[t,s], A. Marinelli[e,f], C. Markou[i], L. Martin[k], J.A. Martínez-Mora[l], F. Marzaioli[u,e], M. Mastrodicasa[ae,g], S. Mastroianni[e], S. Miccichè[w], G. Miele[f,e], P. Migliozzi[e], E. Migneco[w], M.L. Mitsou[e], C.M. Mollo[e], L. Morales-Gallegos[u,e], C. Morley-Wong[al], A. Moussa[y], I. Mozun Mateo[ay,ax], R. Muller[r], M.R. Musone[e,u], M. Musumeci[w], L. Nauta[r], S. Navas[aq], A. Nayerhoda[ak], C.A. Nicolau[g], B. Nkosi[ai], B. Ó Fearraigh[ab,r], V. Oliviero[f,e], A. Orlando[w], E. Oukacha[n], D. Paesani[w], J. Palacios González[c], G. Papalashvili[au], V. Parisi[ap,ad], E.J. Pastor Gomez[c], A. M. Păun[aa], G. E. Păvălaş[aa], S. Peña Martínez[n], M. Perrin-Terrin[d], J. Perronnel[o], V. Pestel[ay], R. Pestes[n], P. Piattelli[w], C. Poirè[z,e], V. Popa[aa], T. Pradier[b], S. Pulvirenti[w], G. Quéméner[o], C. Quiroz[l], U. Rahaman[c], N. Randazzo[a], R. Randriatoamanana[k], S. Razzaque[az], I.C. Rea[e], D. Real[c], S. Reck[ah], G. Riccobene[w], J. Robinson[x], A. Romanov[ap,ad], A. Šaina[c], F. Salesa Greus[c], D.F.E. Samtleben[as,r], A. Sánchez Losa[c,ak], S. Sanfilippo[w], M. Sanguineti[ap,ad], C. Santonastaso[ba,e], D. Santonocito[w], P. Sapienza[w], J. Schnabel[ah], J. Schumann[ah], H. M. Schutte[x], J. Seneca[r], N. Sennan[y], B. Setter[ah], I. Sgura[ak], R. Shanidze[au], Y. Shitov[p], F. Šimkovic[q], A. Simonelli[e], A. Sinopoulou[a], M.V. Smirnov[ah], B. Spisso[e], M. Spurio[t,s], D. Stavropoulos[i], I. Štekl[p], M. Taiuti[ap,ad], Y. Tayalati[m], H. Tedjditi[ad], H. Thiersen[x], I. Tosta e Melo[a,aj], B. Trocmé[n], V. Tsourapis[i], E. Tzamariudaki[i], A. Vacheret[o], V. Valsecchi[w], V. Van Elewyck[aw,n], G. Vannoye[d], G. Vasileiadis[bb], F. Vazquez de Sola[r], C. Verilhac[n], A. Veutro[g,ae], S. Viola[w], D. Vivolo[u,e], J. Wilms[bc], E. de Wolf[ab,r], H. Yepes-Ramirez[l], G. Zarpapis[i], S. Zavatarelli[ad], A. Zegarelli[g,ae], D. Zito[w], J.D. Zornoza[c], J. Zúñiga[c], and N. Zywucka[x].

[a]INFN, Sezione di Catania, Via Santa Sofia 64, Catania, 95123 Italy
[b]Université de Strasbourg, CNRS, IPHC UMR 7178, F-67000 Strasbourg, France
[c]IFIC - Instituto de Física Corpuscular (CSIC - Universitat de València), c/Catedrático José Beltrán, 2, 46980 Paterna, Valencia, Spain
[d]Aix Marseille Univ, CNRS/IN2P3, CPPM, Marseille, France
[e]INFN, Sezione di Napoli, Complesso Universitario di Monte S. Angelo, Via Cintia ed. G, Napoli, 80126 Italy
[f]Università di Napoli “Federico II”, Dip. Scienze Fisiche “E. Pancini”, Complesso Universitario di Monte S. Angelo, Via Cintia ed. G, Napoli, 80126 Italy
[g]INFN, Sezione di Roma, Piazzale Aldo Moro 2, Roma, 00185 Italy
[h]Universitat Politècnica de Catalunya, Laboratori d’Aplicacions Bioacústiques, Centre Tecnològic de Vilanova i la Geltrú, Avda. Rambla Exposició, s/n, Vilanova i la Geltrú, 08800 Spain
[i]NCSR Demokritos, Institute of Nuclear and Particle Physics, Ag. Paraskevi Attikis, Athens, 15310 Greece
[j]University of Granada, Dept. of Computer Architecture and Technology/CITIC, 18071 Granada, Spain
[k]Subatech, IMT Atlantique, IN2P3-CNRS, Université de Nantes, 4 rue Alfred Kastler - La Chantrerie, Nantes, BP 20722 44307 France
[l]Universitat Politècnica de València, Instituto de Investigación para la Gestión Integrada de las Zonas Costeras, C/ Paranimf, 1, Gandia, 46730 Spain
[m]University Mohammed V in Rabat, Faculty of Sciences, 4 av. Ibn Battouta, B.P. 1014, R.P. 10000 Rabat, Morocco
[n]Université Paris Cité, CNRS, Astroparticule et Cosmologie, F-75013 Paris, France
[o]LPC CAEN, Normandie Univ, ENSICAEN, UNICAEN, CNRS/IN2P3, 6 boulevard Maréchal Juin, Caen, 14050 France
[p]Czech Technical University in Prague, Institute of Experimental and Applied Physics, Husova 240/5, Prague, 110 00 Czech Republic
[q]Comenius University in Bratislava, Department of Nuclear Physics and Biophysics, Mlynska dolina F1, Bratislava, 842 48 Slovak Republic
[r]Nikhef, National Institute for Subatomic Physics, PO Box 41882, Amsterdam, 1009 DB Netherlands
[s]INFN, Sezione di Bologna, v.le C. Berti-Pichat, 6/2, Bologna, 40127 Italy
[t]Università di Bologna, Dipartimento di Fisica e Astronomia, v.le C. Berti-Pichat, 6/2, Bologna, 40127 Italy
[u]Università degli Studi della Campania "Luigi Vanvitelli", Dipartimento di Matematica e Fisica, viale Lincoln 5, Caserta, 81100 Italy
[v]E. A. Milne Centre for Astrophysics, University of Hull, Hull, HU6 7RX, United Kingdom

[w]INFN, Laboratori Nazionali del Sud, Via S. Sofia 62, Catania, 95123 Italy
[x]North-West University, Centre for Space Research, Private Bag X6001, Potchefstroom, 2520 South Africa
[y]University Mohammed I, Faculty of Sciences, BV Mohammed VI, B.P. 717, R.P. 60000 Oujda, Morocco
[z]Università di Salerno e INFN Gruppo Collegato di Salerno, Dipartimento di Fisica, Via Giovanni Paolo II 132, Fisciano, 84084 Italy
[aa]ISS, Atomistilor 409, Măgurele, RO-077125 Romania
[ab]University of Amsterdam, Institute of Physics/IHEF, PO Box 94216, Amsterdam, 1090 GE Netherlands
[ac]TNO, Technical Sciences, PO Box 155, Delft, 2600 AD Netherlands
[ad]INFN, Sezione di Genova, Via Dodecaneso 33, Genova, 16146 Italy
[ae]Università La Sapienza, Dipartimento di Fisica, Piazzale Aldo Moro 2, Roma, 00185 Italy
[af]Università di Bologna, Dipartimento di Ingegneria dell'Energia Elettrica e dell'Informazione "Guglielmo Marconi", Via dell'Università 50, Cesena, 47521 Italia
[ag]Cadi Ayyad University, Physics Department, Faculty of Science Semlalia, Av. My Abdellah, P.O.B. 2390, Marrakech, 40000 Morocco
[ah]Friedrich-Alexander-Universität Erlangen-Nürnberg (FAU), Erlangen Centre for Astroparticle Physics, Nikolaus-Fiebiger-Straße 2, 91058 Erlangen, Germany
[ai]University of the Witwatersrand, School of Physics, Private Bag 3, Johannesburg, Wits 2050 South Africa
[aj]Università di Catania, Dipartimento di Fisica e Astronomia "Ettore Majorana", Via Santa Sofia 64, Catania, 95123 Italy
[ak]INFN, Sezione di Bari, via Orabona, 4, Bari, 70125 Italy
[al]International Centre for Radio Astronomy Research, Curtin University, Bentley, WA 6102, Australia
[am]University Würzburg, Emil-Fischer-Straße 31, Würzburg, 97074 Germany
[an]Western Sydney University, School of Computing, Engineering and Mathematics, Locked Bag 1797, Penrith, NSW 2751 Australia
[ao]IN2P3, LPC, Campus des Cézeaux 24, avenue des Landais BP 80026, Aubière Cedex, 63171 France
[ap]Università di Genova, Via Dodecaneso 33, Genova, 16146 Italy
[aq]University of Granada, Dpto. de Física Teórica y del Cosmos & C.A.F.P.E., 18071 Granada, Spain
[ar]NIOZ (Royal Netherlands Institute for Sea Research), PO Box 59, Den Burg, Texel, 1790 AB, the Netherlands
[as]Leiden University, Leiden Institute of Physics, PO Box 9504, Leiden, 2300 RA Netherlands
[at]National Centre for Nuclear Research, 02-093 Warsaw, Poland
[au]Tbilisi State University, Department of Physics, 3, Chavchavadze Ave., Tbilisi, 0179 Georgia
[av]The University of Georgia, Institute of Physics, Kostava str. 77, Tbilisi, 0171 Georgia
[aw]Institut Universitaire de France, 1 rue Descartes, Paris, 75005 France
[ax]IN2P3, 3, Rue Michel-Ange, Paris 16, 75794 France
[ay]LPC, Campus des Cézeaux 24, avenue des Landais BP 80026, Aubière Cedex, 63171 France
[az]University of Johannesburg, Department Physics, PO Box 524, Auckland Park, 2006 South Africa
[ba]Università degli Studi della Campania "Luigi Vanvitelli", CAPACITY, Laboratorio CIRCE - Dip. Di Matematica e Fisica - Viale Carlo III di Borbone 153, San Nicola La Strada, 81020 Italy
[bb]Laboratoire Univers et Particules de Montpellier, Place Eugène Bataillon - CC 72, Montpellier Cédex 05, 34095 France
[bc]Friedrich-Alexander-Universität Erlangen-Nürnberg (FAU), Remeis Sternwarte, Sternwartstraße 7, 96049 Bamberg, Germany
[bd]Université de Haute Alsace, rue des Frères Lumière, 68093 Mulhouse Cedex, France
[be]AstroCeNT, Nicolaus Copernicus Astronomical Center, Polish Academy of Sciences, Rektorska 4, Warsaw, 00-614 Poland

Acknowledgements

The authors acknowledge the financial support of the funding agencies: Agence Nationale de la Recherche (contract ANR-15-CE31-0020), Centre National de la Recherche Scientifique (CNRS), Commission Européenne (FEDER fund and Marie Curie Program), LabEx UnivEarthS (ANR-10-LABX-0023 and ANR-18-IDEX-0001), Paris Île-de-France Region, France; Shota Rustaveli National Science Foundation of Georgia (SRNSFG, FR-22-13708), Georgia; The General Secretariat of Research and Innovation (GSRI), Greece Istituto Nazionale di Fisica Nucleare (INFN), Ministero dell'Università e della Ricerca (MIUR), PRIN 2017 program (Grant NAT-NET 2017W4HA7S) Italy; Ministry of Higher Education, Scientific Research and Innovation, Morocco, and the Arab Fund for Economic and Social Development, Kuwait; Nederlandse organisatie voor Wetenschappelijk Onderzoek (NWO), the Netherlands; The National Science Centre, Poland (2021/41/N/ST2/01177); The grant "AstroCeNT: Particle Astrophysics Science and Technology Centre", carried out within the International Research Agendas programme of the Foundation for Polish Science financed by the European Union under the European Regional Development Fund; National Authority for Scientific Research (ANCS), Romania; Grants PID2021-124591NB-C41, -C42, -C43 funded by MCIN/AEI/ 10.13039/501100011033 and, as appropriate, by "ERDF A way of making Europe", by the "European Union" or by the "European Union NextGenerationEU/PRTR", Programa de Planes Complementarios I+D+I (refs. ASFAE/2022/023, ASFAE/2022/014), Programa Prometeo (PROMETEO/2020/019) and GenT (refs. CIDEGENT/2018/034, /2019/043, /2020/049. /2021/23) of the Generalitat Valenciana, Junta de Andalucía (ref. SOMM17/6104/UGR, P18-FR-5057), EU: MSC program (ref. 101025085), Programa María Zambrano (Spanish Ministry of Universities, funded by the European Union, NextGenerationEU), Spain; The European Union's Horizon 2020 Research and Innovation Programme (ChETEC-INFRA - Project no. 101008324).